RESEARCH ARTICLE

A New Platform of B/N-Doped Cyclophanes: Access to π-Conjugated Block-Type B_3N_3 Macrocycle with Strong Dipole Moment and Unique Optoelectronic Properties

Pengfei Li,[a] Daisuke Shimoyama,[c] Niu Zhang,*[b] Yawei Jia,[a] Guofei Hu,[a] Chenglong Li,[a] Xiaodong Yin,[a] Nan Wang,[a] Frieder Jäkle,*[c] and Pangkuan Chen*[a]

[a] P. Li, Y. Jia, G. Hu, C. Li, Dr. X. Yin, Dr. N. Wang, Prof. Dr. P. Chen
Beijing Key Laboratory of Photoelectronic/Electrophotonic Conversion Materials, Key Laboratory of Cluster Science of the Ministry of Education, School of Chemistry and Chemical Engineering, Beijing Institute of Technology of China
Beijing, 102488 (China)
E-mail: pangkuan@bit.edu.cn

[b] Dr. N. Zhang
Analysis & Testing Centers, Beijing Institute of Technology of China
Beijing, 102488 (China)
E-mail: niuzhang2019@bit.edu.cn

[c] Dr. D. Shimoyama, Prof. Dr. F. Jäkle
Department of Chemistry, Rutgers University-Newark, 73 Warren Street, Newark, NJ, 07102, USA
E-mail: fjaekle@newark.rutgers.edu

Abstract: We herein describe a new design principle to achieve B/N-doped cyclophane where an electron-donor block of three triarylamines (Ar_3N) and acceptor block of three triarylboranes (Ar_3B) are spatially separated on opposite sides of the π-extended ring system. DFT computations revealed the distinct electronic structure of the *block*-type macrocycle **MC-*b*-B3N3** with a greatly enhanced dipole moment and reduced HOMO-LUMO energy gap in comparison to its analogue with alternating B and N sites, **MC-*alt*-B3N3**. The unique arrangement of borane acceptor Ar_3B and amine donor Ar_3N components in **MC-*b*-B3N3** induces exceptionally strong intramolecular charge transfer in the excited state, which is reflected in a largely red-shifted luminescence at 612 nm in solution. The respective linear open-chain oligomer **L-*b*-B3N3** was also synthesized for comparison. Our new approach to donor-acceptor macrocycles offers important fundamental insights and opens up a new avenue to unique optoelectronic materials.

Introduction

As synthetically challenging but frequent targets, macrocyclic architectures have inspired tremendous synthetic efforts that have recently been redoubled due to their great potential for applications in host-guest chemistry,[1] supramolecular assembly[2] and materials science.[3] Well-defined cyclic π-systems exhibit electronically distinct π-conjugation effects that result in unique structure-dependent electronic, optical and magnetic characteristics.[4] Notwithstanding significant advances over the past few years, from the perspective of synthetic access, great challenges still remain because cyclization tends to be thermodynamically unfavorable as a result of the intrinsic strain energies which in turn leads to low yields. The development of a universal approach to cyclize modular systems with highly scalable synthesis and structure-tunable properties is central to the strategic design of these emerging materials. In view of the dominant role played by ring strain, the proposed topology and selected building blocks considerably dictate the ability to successfully construct the rigid macrocyclic π skeletons. In search of such systems non-strained cyclic hexamers with subunits consisting of linear π-systems separated by sp^2-hybridized electron donors (D) and/or acceptors (A) are emerging as promising targets. Four different arrangements are conceivable: (I) electron-rich D6, (II) electron-deficient A6, (III) ambipolar D3A3 with alternating D/A, and (IV) *block*-type D3A3 macrocycles (Scheme 1). These macrocycles are electronically distinct, and the relative alignment of D and A moieties is expected to play a key role in tuning the electronic properties.

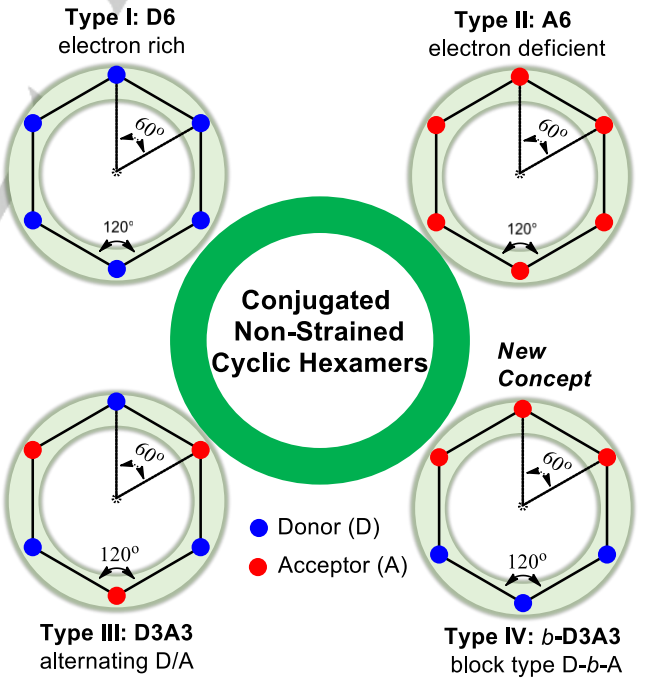

Scheme 1. Conceptual diagram illustrating new platform in comparison with typical arrangement of electron-rich donor (D) and electron-deficient acceptors (A) in hexameric bora- and azacyclophanes.

Main group heteroatom doping has proven particularly advantageous for the modulation of the electronic structure and physicochemical characteristics of conjugated π-systems.[5] Thus, electron-deficient triarylborane acceptor (Ar_3B) and electron-rich triarylamine donor (Ar_3N) functionalities are frequently employed

to tune the photophysical properties of conjugated materials.[6] As illustrated in Scheme 2, the synthesis of electron-rich arylamine-based azacyclophane **MC-N6-Phen** (I) was first reported by Ito, Tanaka and co-workers.[7] The Jäkle group has pioneered B-doped cyclophanes **MC-B6-Flu** and **MC-B6-Phen** (II) as electron-deficient analogues, as well as introduced an ambipolar hexamer **MC-*alt*-B3N3** (III).[8] However, closer inspection reveals that all of these intriguing macrocycles are highly symmetric and exhibit a dipole moment of $\mu = 0$ in the ground state. In view of the potential applications in ferroelectrics,[9] nonlinear optics[10] and optoelectronic devices with improved charge separation,[11] herein we propose *block*-type architectures as a new design principle for π-conjugated macrocycles with large dipole moments and low HOMO-LUMO gaps. In comparison to cyclophanes of type I, II and III, *block*-type systems of type IV may give rise to exceptional properties that are inaccessible from traditional conjugated macrocycles. Indeed, computational analyses predict that *block*-type macrocycles display greatly enhanced dipole moments, as a result of the spatial separation of an acceptor block and a donor block in the π-conjugated hexamer scaffold (Scheme 2, IV). Thus, the successful synthesis of **MC-*b*-B3N3** offers a promising new direction in this field while shedding some light on relevant fundamentals and future applications.

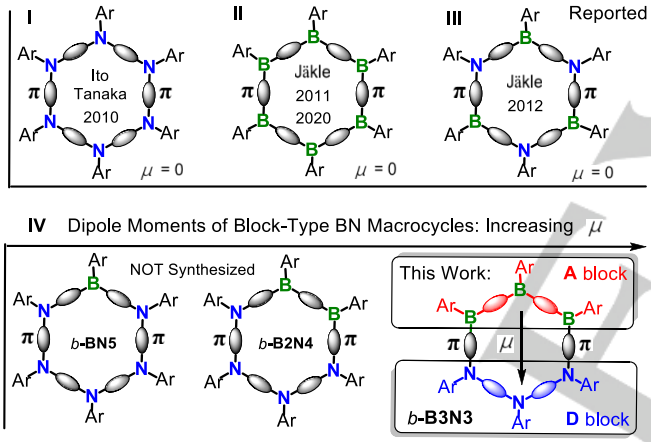

Scheme 2. Representative structures of B/N doped cyclic hexamers with aromatic spacers in a π–extended skeleton.

Results and Discussion

The synthetic pathways to cyclic **MC-*b*-B3N3** and open-chain **L-*b*-B3N3** are shown in Scheme 3 and the Supporting Information (SI). The synthesis of intermediate **1** started from $TipB(OMe)_2$ (Tip = 2,4,6-triisopropylphenyl) as the boron source, and the number of the boron sites was then increased by highly selective Si/B exchange reaction between **1** and BBr_3 to give **2**. Extension of π-conjugation in the electron-donating block was readily achieved *via* iterative C-N coupling reactions.[5o] With these precursors in hand, the electron donor and acceptor block were coupled via a Sn/B exchange reaction to generate the macrocyclic architecture. The resulting acceptor block (B3) was subsequently stabilized with sterically hindered Tip groups to give rise to the targeted **MC-*b*-B3N3** in 20% overall yield from **1**.

After standard reaction workup and further purification by preparative column chromatography, the cyclic product was fully characterized by ^1H, ^{13}C, ^{11}B NMR and HRMS. As shown in Figure

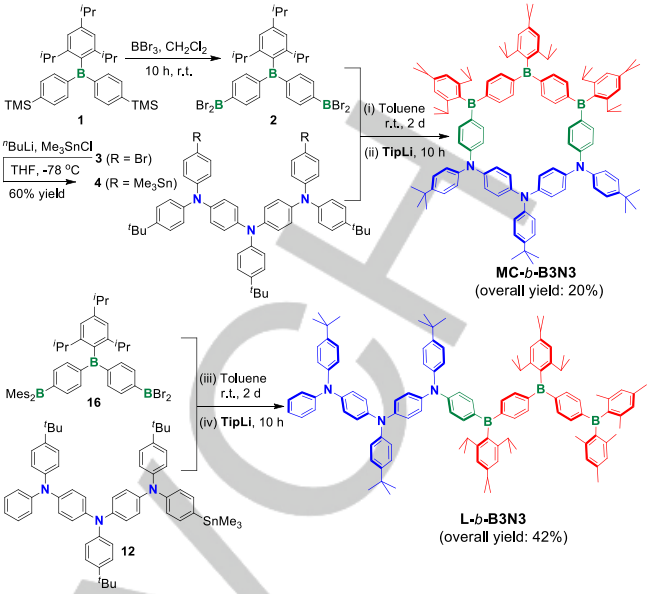

Scheme 3. Key steps in the synthesis of **MC-*b*-B3N3** and **L-*b*-B3N3**; Tip = 2,4,6-triisopropylphenyl.

1a, two low-field doublets at $\delta = 7.9$ ppm in the ^1H NMR spectrum (C_6D_6, 25 °C) can be assigned to the aromatic protons (H_a and H_b) adjacent to electron-deficient B centers. Similarly, due to the deshielding effect of B, the doublet peak at $\delta = 7.7$ ppm should correspond to protons H_c. The aromatic protons assigned to the electron-donor block of the triarylamine subunits were shifted to higher field and some of these signals overlap. The boron centers are in two distinct environments, giving rise to very broad overlapped ^{11}B NMR resonances in the range of $\delta = 60$–80 ppm, which is consistent with the presence of sp^2-hybridized borons. When the sample was heated to 70 ºC a relatively sharper signal emerged at $\delta = 74$ ppm. The successful access to the new macrocycle **MC-*b*-B3N3** was further confirmed by high-resolution MALDI-TOF-MS (Figure 1b and S1), which gave a single peak at *m/z* 1540.0753 corresponding to the molecular ion (calcd 1540.0736).

MC-*b*-B3N3 exhibited reasonably high tolerance to air in the solid state without any decomposition over a period of several hours and proved to be thermally stable up to >200 °C (Figure S29d). The electronic properties of **MC-*b*-B3N3** and **L-*b*-B3N3** were explored by UV-Vis absorption and emission spectroscopy. As shown in Figure 2a, **MC-*b*-B3N3** and **L-*b*-B3N3** displayed a main absorption band at 346 and 328 nm, respectively, likely assigned to charge transfer from the protecting Tip groups to B3 segments (see Figure 3d: $S_0 \rightarrow S_4$ and S_5). The relatively less intense shoulder peaks at $\lambda_{abs} = 416$ and 423 nm in the absorption spectra correspond to lower-energy transitions that can be ascribed to intramolecular charge transfer (ICT) from the electron-donor block (-N-π-N-π-N-) to the acceptor block (-B-π-B-π-B-) (i.e., transitions $S_0 \rightarrow S_1$, S_2 and S_3). The optical energy gaps of $E_{gap(optical)} = 2.51$ and 2.48 eV for **MC-*b*-B3N3** and **L-*b*-B3N3** agree well with the computational results ($E_{gap(DFT)}$: 2.60 and 2.47 eV, Table 1 and SI). Both *block*-type molecules were found to be highly luminescent in non-coordinating and non-chlorinated organic solvents (Table S2 and S3). They show an apparent bathochromic shift in the emission spectra with increasing solvent polarity as the result of their donor-acceptor character (Figure S29 and S35).

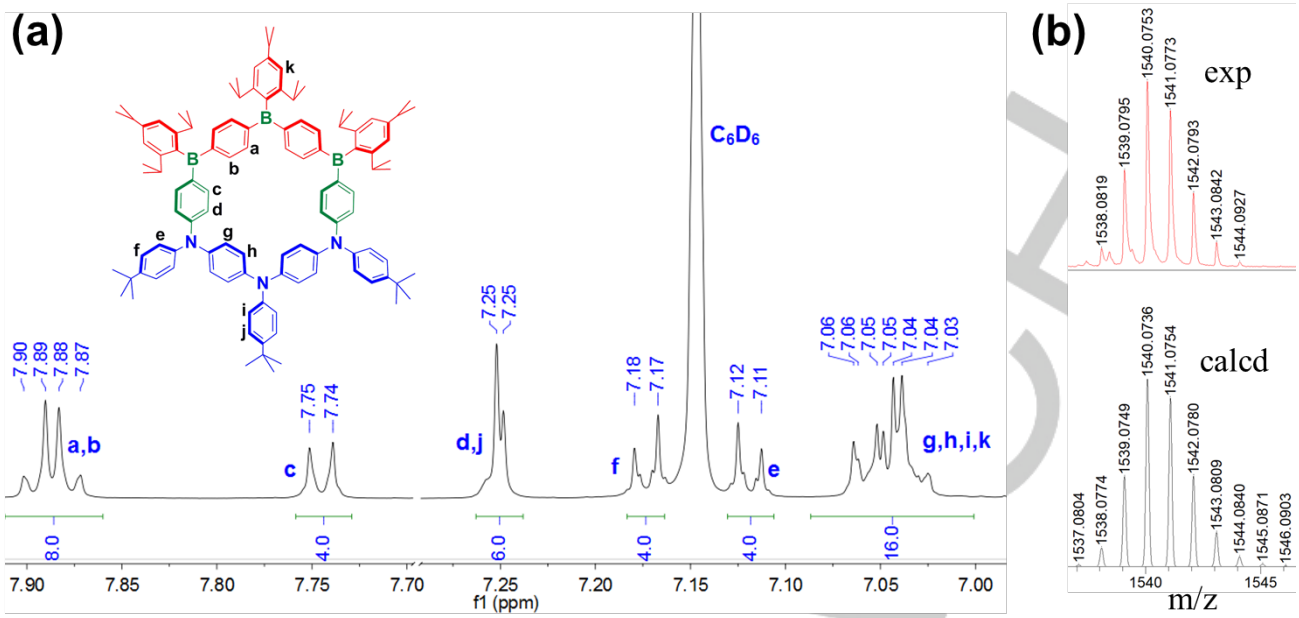

Figure 1. (a) Aromatic region of the ^{1}H NMR spectrum of **MC-*b*-B3N3** (700 MHz, C_6D_6, 25 °C). (b) MALDI-TOF mass spectrum (positive ion mode) of **MC-*b*-B3N3** showing experimental and simulated isotopic patterns.

Surprisingly, under ambient conditions both compounds show a strong orange emission in solution (**MC-*b*-B3N3**: 612 nm; **L-*b*-B3N3**: 592 nm, toluene) as well as in the solid state (**MC-*b*-B3N3**: 582 nm, Φ_S = 0.17; **L-*b*-B3N3**: 586 nm, Φ_S = 0.17). The quantum yield in hexane is particularly high (**MC-*b*-B3N3**: Φ_L = 0.80, τ = 17 ns; **L-*b*-B3N3**: Φ_L = 0.85, τ = 10 ns, see Table S2 and S3). In comparison, the previously reported cyclic hexamers **MC-B6-Flu**, **MC-B6-Phen**, and **MC-*alt*-B3N3** all emit blue light (< 460 nm, Table 1), and the emission maximum of the *block*-type macrocycle **MC-*b*-B3N3** is greatly red-shifted by over 150 nm relative to its isomer **MC-*alt*-B3N3**. This remarkable redshift for **MC-*b*-B3N3** is attributed to the unique electronic structure that results from the peculiar combination of electron donors and acceptors. Both the electron-donating and accepting strength are considerably enhanced for **MC-*b*-B3N3** because three Ar_3N and Ar_3B moieties are arranged in separate blocks. The unique photophysical properties are then enabled by the strong electronic interactions in the *block*-type system.

On account of computational results, cyclic D3A3 *diblock* hexamers in general exhibit more polar structures and narrower HOMO-LUMO energy gaps in comparison to other arrangements (e.g., electron-deficient **MC-B6** and alternating ambipolar **MC-*alt*-B3N3**, μ_g = 0.00 D). Among *block*-type cyclic hexamers, the calculated dipole moment (μ_g) increases and the E_{gap} decreases in the order of *b*-**BN5**, *b*-**B2N4** and *b*-**B3N3** (Figure S44). The Janus-type electronic structure of **MC-*b*-B3N3** could be visualized in an electrostatic potential (ESP) map. As shown in Figure 3a-c, a comparison of the ESP maps for three types of macrocycles revealed that the negative charges are distributed on the electron-donating arylamine block, while the electron-accepting arylborane block is positively charged, leading to the considerably large dipole moment in **MC-*b*-B3N3** (μ_g = 3.17 D).

The electronic structure of **MC-*b*-B3N3** was further examined using DFT (B3LYP/CAM-B3LYP, 6-31G*) and TD-DFT (B3LYP/CAM-B3LYP, 6-311G**) methods. As anticipated, the HOMO is delocalized over the electron-rich donor block with a

Table 1. Comparison of the photophysical, computational and electrochemical data for **MC-*b*-B3N3**, **L-*b*-B3N3** and related boracyclophanes.

	λ_{abs}[a] (nm)	λ_{em}[a] (nm)	Φ_L[b] (%)	τ_{av}[c] (ns)	$E_{gap(DFT)}$[d] (eV)	E_{TDDFT}[e] (eV)	$E_{gap(optical)}$[f] (eV)	$E^{ox1}_{1/2}$[g] (V)	$E^{red1}_{1/2}$[g] (V)	$E_{gap(elec)}$ (eV)
MC-*b*-B3N3	416	612	11	4	2.60	2.30	2.51	+0.02	–2.10	2.12
L-*b*-B3N3	423	592	18	2	2.47	2.23	2.48	–0.01	–2.04	2.03
MC-N6-Phen[h]	348	–	–	–	–	–	–	–0.28	–	–
MC-B6-Flu[i]	366	425	–	–	3.49	–	–	–	–2.10	–
MC-B6-Phen[j]	302	427	–	–	4.11	–	–	–	–1.56	–
MC-*alt*-B3N3[k]	420	460	–	–	3.32	–	–	+0.46	–2.53	2.99

[a] Recorded in toluene (c = 1.0 × 10^{-5} M). [b] Emission quantum efficiency (Φ_L) measured in toluene. [c] Emission lifetime (τ_{av}) in toluene. [d] Energy gaps: E_{gap} = E_{LUMO} – E_{HOMO} obtained by DFT calculation (B3LYP, 6-31G*). [e] Vertical excitation of the lowest transition ($S_0 \rightarrow S_1$) calculated by TD-DFT (B3LYP, 6-311G**). [f] $E_{gap(optical)}$: experimental optical energy gap obtained from the onset of absorption spectra in toluene. [g] $E^{ox1}_{1/2}$ and $E^{red1}_{1/2}$: half-wave potential of oxidation and reduction in CH_2Cl_2 determined by cyclic voltammetry (*vs* Fc^+/Fc). [h] Ref 8c. [i] Ref 7. [j] Ref 8a. [k] Ref 8b.

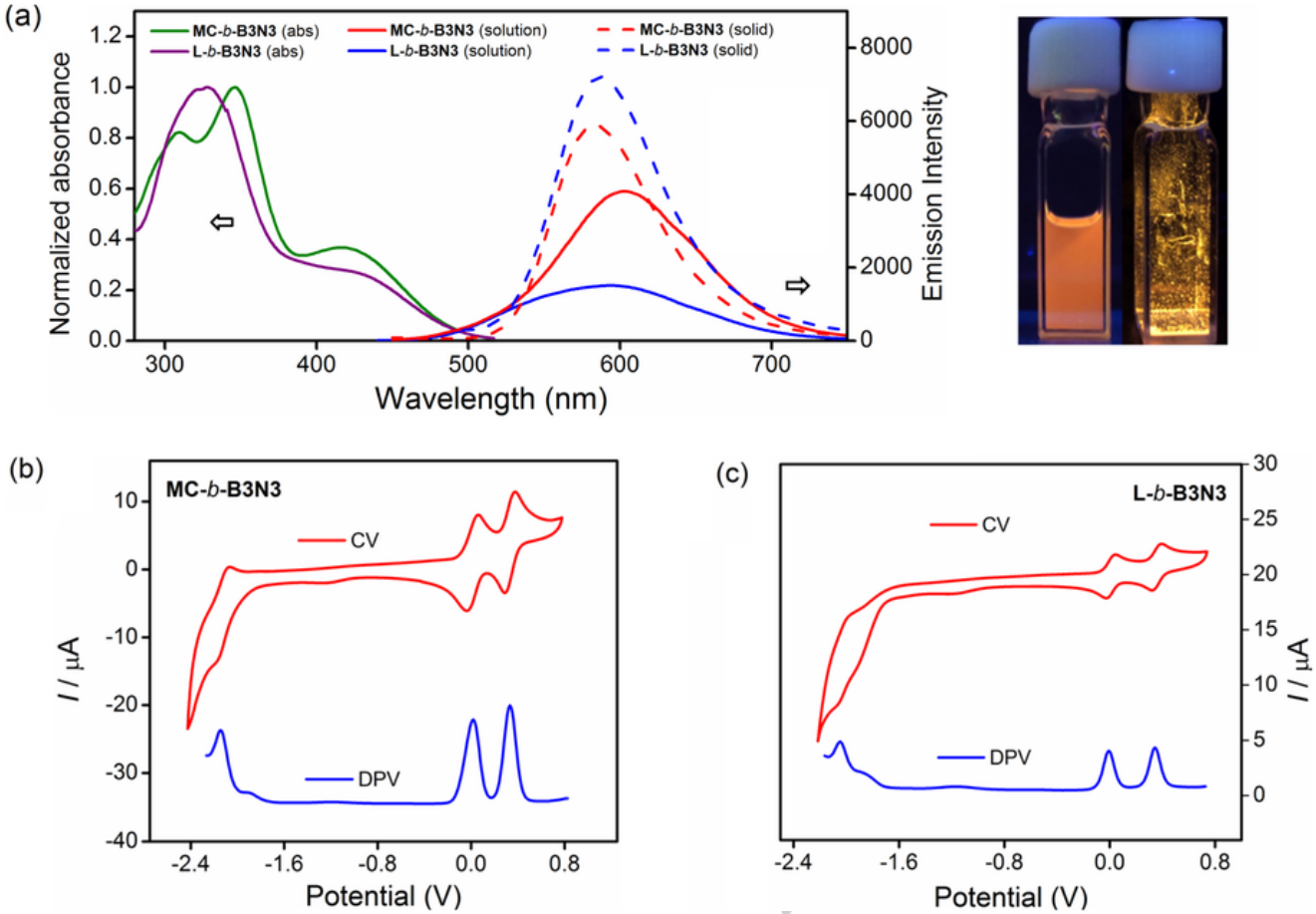

Figure 2. (a) UV-Vis absorption and emission spectra of **MC-*b*-B3N3** (λ_{ex} = 416 nm) and **L-*b*-B3N3** (λ_{ex} = 423 nm) in toluene (c = 1.0 × 10^{-5} M). Inset: photographs of emission colors of **MC-*b*-B3N3** in toluene and in the solid state under 365 nm UV irradiation. (b,c) Cyclic and differential pulse voltammetry (CV and DPV) curves (*vs* Fc^+/Fc) in CH_2Cl_2, using *n*-Bu_4NPF_6 (0.1 M) as the electrolyte, v = 100 mV/s.

strong contribution from the aromatic pendent groups on N, whereas the LUMO (–2.02 eV) is delocalized over the electron-acceptor block, involving only the B atoms and π-linkers within the cyclic skeleton (Figure 3d). Compared with other hexamer analogues, the HOMO-LUMO energy gaps are dramatically reduced in *block*-type systems and that of **MC-*b*-B3N3** is the smallest with $E_{gap(DFT)}$ = 2.60 eV. The three lowest energy transitions to S_1, S_2 and S_3 are dominated by charge transfer from the donor block to the acceptor block, along with a moderate π–π* contributions of the two bridging phenyl rings. Higher energy transitions ($S_0 \rightarrow S_4$ and S_5) can be assigned to vertical excitations to the LUMO from the degenerate HOMO-3, HOMO-4 and HOMO-5, involving charge transfer from the electron-rich exocyclic Tip substituents to the acceptor block. Notably, the polar structure of *block*-type **MC-*b*-B3N3** renders the lowest-energy transition symmetry-allowed ($S_0 \rightarrow S_1$, f = 0.2225), in stark contrast to the case of highly symmetric macrocycles such as **MC-*alt*-B3N3**, for which the lowest energy transitions are symmetry-forbidden.[6a,8]

MC-*b*-B3N3 and **L-*b*-B3N3** were further characterized by cyclic voltammetry (CV) and differential pulse voltammetry (DPV) (Figure 2b and 2c). For **MC-*b*-B3N3**, two reversible oxidation waves at $E^{ox}_{1/2}$ = 0.02 V and 0.33 V relative to the ferrocene/ferrocenium redox couple (Fc/Fc^+) were observed in CH_2Cl_2 and can be assigned to the oxidation of two of the three triarylamine moieties (the third oxidation wave is outside the electrochemical window).[5o] Similar oxidation processes were also observed for **L-*b*-B3N3**, but at a slightly lower potential of –0.01 and 0.34 V. Only the first electrochemical reduction of the triarylborane moieties could be observed, which occurred at $E^{red}_{1/2}$ = –2.10 V in **MC-*b*-B3N3** and at a slightly higher potential of $E^{red1}_{1/2}$ = –2.04 V for **L-*b*-B3N3**. These processes are attributed to preferential reduction of the central boron atom that is surrounded by electron-deficient borylated phenyl group. Additional reductions at the outer boron centers could not be observed within the electrochemical window, because of the expected strong coulombic interactions and the electron-donating effect of the attached amino-substituted phenyl groups. The subtle differences in redox chemistry could be related to more effective delocalization of π-conjugated electron-donor and acceptor blocks in the cyclic in comparison to the more flexible linear structure.

As seen in Table 1, compared with the electron-rich macrocycle **MC-N6-Phen** reported by Ito and Tanaka, the *block*-type **MC-*b*-B3N3** is slightly less readily oxidized ($E^{ox1}_{1/2}$: 0.02 *vs* –0.28 V) due to the imbedded electron-acceptor block. Relative to Jäkle's fluoromesityl-substituted hexabora-cyclophane **MC-B6-Phen** ($E^{red1}_{1/2}$ = –1.56 V), the reduction potential of **MC-*b*-B3N3** at $E^{red}_{1/2}$ = –2.10 is more negative, but it is similar to that for **MC-B6-Flu** with its longer fluorene linkers ($E^{red1}_{1/2}$ = –2.10 V). For the ambipolar **MC-*alt*-B3N3**, in which electron-rich triarylamines alternate with electron-deficient triarylboranes, the first oxidation and reduction waves were observed at $E^{ox1}_{1/2}$ = 0.46 V and

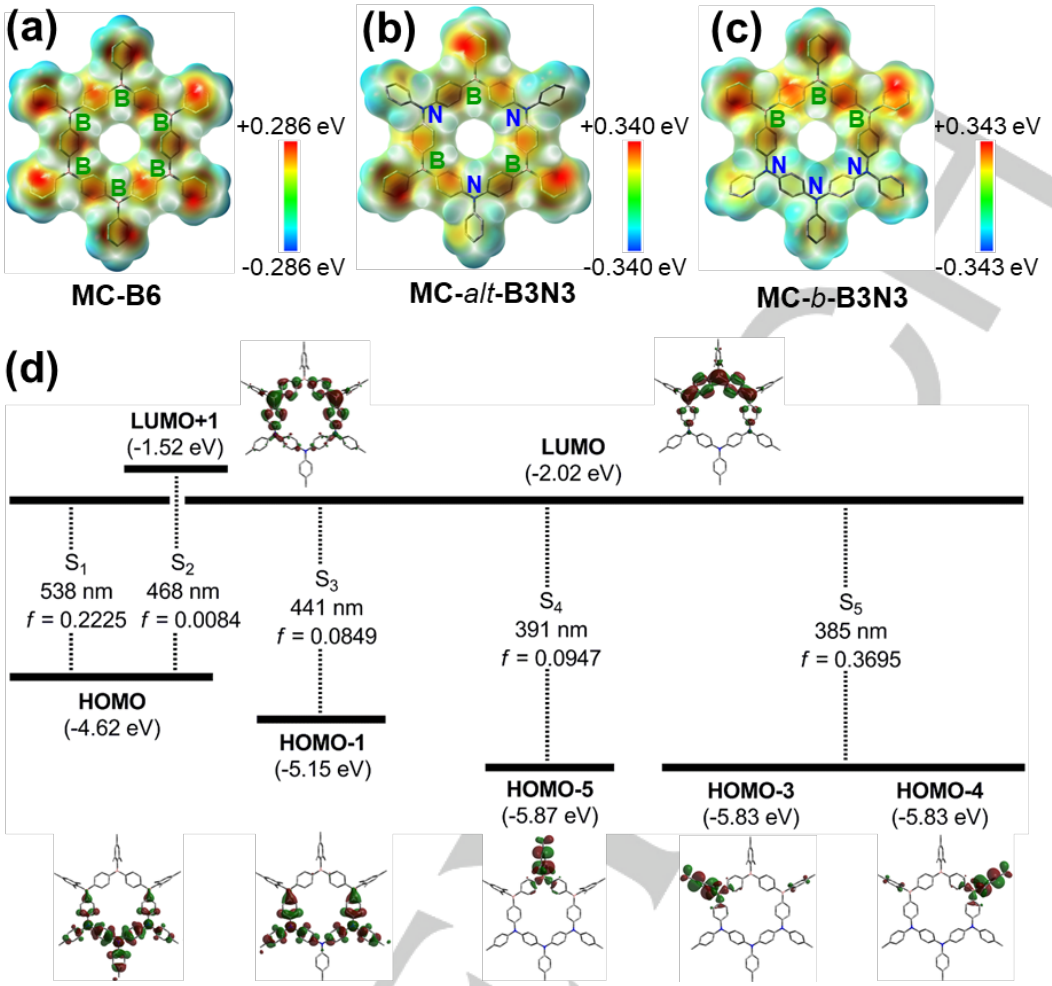

Figure 3. (a,b,c) Calculated electrostatic potentials (ESP) mapped onto the electron density isosurfaces of simplified model systems **MC-B6** (D_{3d}), **MC-*alt*-B3N3** (D_3) and **MC-*b*-B3N3** (C_2) with all substituents replaced by H. (d) Key electronic transitions contributing to vertical excitations of simplified **MC-*b*-B3N3** (TD-DFT, B3LYP/6-311G**) with molecular orbital plots (iso = 0.02, B3LYP/6-31G*). The *iso*-propyl and *t*-butyl groups are simplified as Me groups.

$E^{red1}_{1/2}$ = –2.53 V, respectively. In comparison to this analogue, the *block*-type **MC-*b*-B3N3** is considerably easier to oxidize or reduce. The electrochemical energy gap of 2.12 eV for **MC-*b*-B3N3** is much lower than that of other cyclic hexamers in line with the trends indicated by computational studies. These results indicate that **MC-*b*-B3N3** should be more susceptible to electrochemical stimuli and could be a promising candidate for applications in redox-active materials.

Given the prominent electron-deficient character endowed by the Lewis acidic triarylboranes specifically arranged in a single acceptor block, we also explored the anion binding behavior of **MC-*b*-B3N3** by titration with tetrabutylammonium fluoride (TBAF). As shown in Figure 4a, the addition of fluoride to a solution of **MC-*b*-B3N3** in toluene led to a gradual decrease of the longest wavelength absorption at 416 nm, assigned to charge transfer between the two blocks, and a new band developed at 375 nm in the early stages of the titration. The further attenuation of the band at 375 nm in the presence of a 10-fold excess of fluoride indicated that the borons in the macrocycle were fully converted to electron-rich tetracoordinate borate species, thereby eliminating the charge transfer processes. Complexation of **MC-*b*-B3N3** with excess fluoride anions was spectroscopically confirmed by an upfield shift from δ = 67 to 6 ppm in ^{11}B NMR spectra (Figure S33).

Fitting of the absorption titration data resulted in three binding constants ($\lg\beta_{11}$ = 5.8, $\lg\beta_{12}$ = 10.2, $\lg\beta_{13}$ = 13.5) corresponding to 3 separate binding events (Figure S31 and S32). The first binding of fluoride is expected to occur preferentially at the boron center that is surrounded by electron-withdrawing borylated phenyl rings, whereas the second binding of fluoride would likely be favored at the borons that are not attached to the same phenylene ring to minimize coulombic repulsion (requiring a simultaneous electron transfer from the central to one of the outer borons).[12] The linear species **L-*b*-B3N3** showed a similar anion binding property but with slightly reduced binding strength ($\lg\beta_{11}$ = 5.3, $\lg\beta_{12}$ = 9.1, $\lg\beta_{13}$ = 12.7) compared with **MC-*b*-B3N3** (Figure 4b and S37). This observation was further elucidated by the presence of NMR signals at δ_B = 7 and 70 ppm as a major and minor resonance, respectively (Figure S36, S38 and S39). Upon complexation of the electron-acceptor block of **MC-*b*-B3N3**, the orange emission at 612 nm was quenched, gradually giving rise to a higher-energy emission band at λ_{em} = 525 nm, followed by emergence of a further blue-shifted band at 435 nm that is attributed to locally excited π-π^* transitions (Figure 4c). Similarly, upon fluoride complexation **L-*b*-B3N3** experienced a strongly enhanced emission with a spectral shift from 592 to 515 nm. At higher F^- concentration the band at 515 nm shifted further and split into two

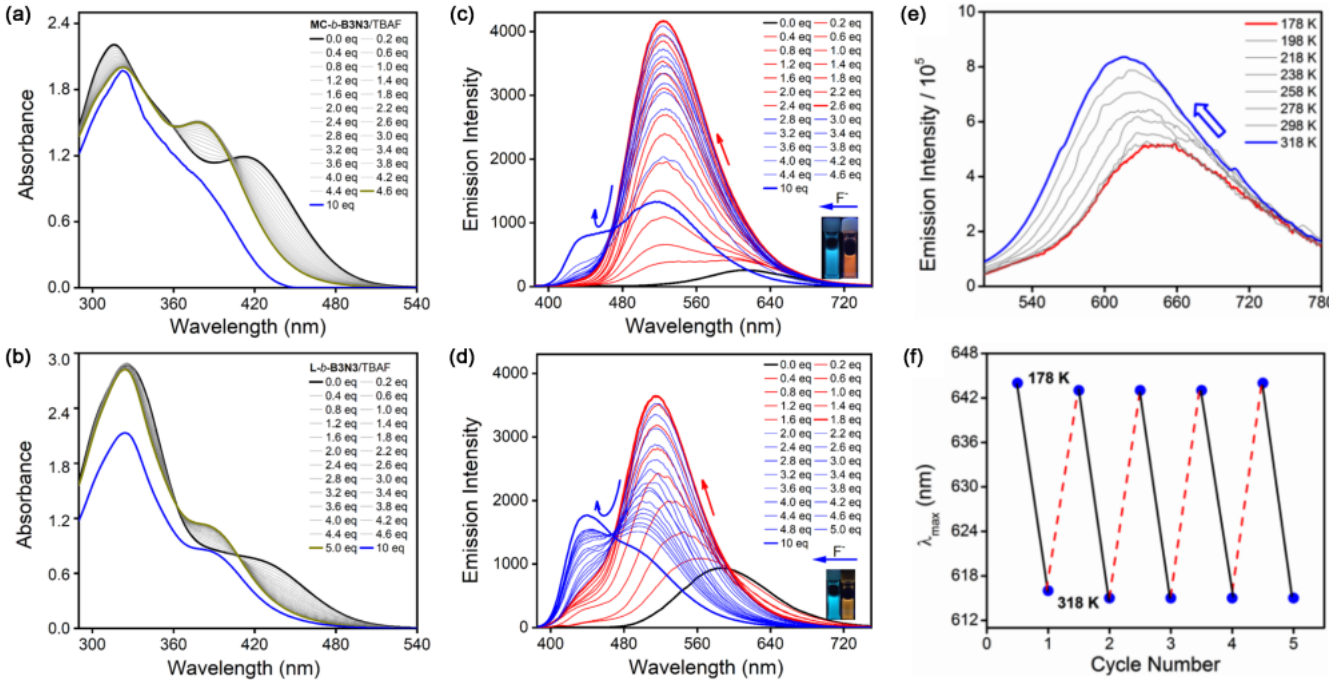

Figure 4. (a, b) UV-Vis absorption and (c, d) emission spectra for **MC**-*b*-**B3N3** (c = 5.0 × 10^{-5} M, λ_{ex} = 360 nm) and **L**-*b*-**B3N3** (c = 6.35 × 10^{-5} M, λ_{ex} = 360 nm) in toluene as an immediate addition of TBAF. (e) Temperature-dependent emission spectra for **MC**-*b*-**B3N3** in toluene (c = 1.0 × 10^{-5} M, λ_{ex} = 416 nm) between 178 K and 318 K. (f) Reversible emission modulation by temperature cycling of **MC**-*b*-**B3N3**.

bands at ca. 500 and 440 nm. Finally, a gradual decrease in the band at 500 nm and an increase in the band at λ_{em} = 440 were detected (Figure 4d).[13] The changes in the emission wavelength for **MC**-*b*-**B3N3** and **L**-*b*-**B3N3** with increasing F^- concentration are consistent with initial formation of partially complexed species that exhibit ICT bands at shorter wavelength than the uncomplexed species, which gradually are superseded by a high energy emission due to π-π* transitions of the fully complexed species (Figure S32). The responses to complexation of **MC**-*b*-**B3N3** and **L**-*b*-**B3N3** with fluoride are suggestive of possible applications in luminescent switches induced by host-guest chemistry.

Variable-temperature emission spectra demonstrated that **MC**-*b*-**B3N3** also responds to changes in temperature as an external stimulus (Figure 4e，S34). As shown in Figure 4e, the emission maximum of **MC**-*b*-**B3N3** experienced a bathochromic shift of 30 nm when the temperature increased from 178 to 318 K. This thermochromic response was reversible and displayed a marked fatigue resistance as indicated by 5 cycles of alternating temperature without emission degradation (Figure 4f). A similar behavior was also observed for **L**-*b*-**B3N3** (Figure S40). The thermally-induced bathochromic shifts of the emission in these structurally unique donor-acceptor systems are proposed to derive from the stabilization of the ICT state, which in turn is related to the temperature-dependence of the solvent polarity.[6p]

The above-unraveled characteristics for the new *block*-type **MC**-*b*-**B3N3** have established a conceptually unique donor-acceptor charge transfer system that is different from previous efforts to build π-conjugated main group macrocycles. We anticipate that the first-ever development of these types of *block*-type macrocyclic systems would spark interest in this nascent realm and inspire further exploration as new scaffolds for high-performance electronics, ferroelectrics, and nanotubular assembly; the latter taking advantage of their higher symmetry and the preferable 3D-disposed organization, in sharp contrast to the well-known open-structured *block* co-oligomers and polymers.

Conclusion

We herein reported on the design principle and synthetic approach to a new class of π-conjugated macrocycle with unique architectures and electronic structures. Motivated by the great potential of π-electron-delocalized hexamers as attractive non-strained cyclophanes, we proposed a readily accessible macrocyclic system composed of charge-reversed electron-donor and electron-acceptor blocks. We have achieved the synthesis of the first *block*-type macrocycle **MC**-*b*-**B3N3** by stitching together a π-expanded donor block and an acceptor block within a cyclic backbone. The electronic structure of this cyclic π-system is unique and fundamentally different from those of other cyclic hexamer analogues such as **MC-N6-Phen**, **MC-B6-Flu**, **MC-B6-Phen** and **MC**-*alt*-**B3N3**. **MC**-*b*-**B3N3** shows a dipolar cyclic framework with a narrow HOMO-LUMO energy gap, as evidenced by a strongly red-shifted orange emission at 612 nm and a small $E_{gap(elec)}$ of 2.12 eV. The highly efficient low-energy emission, together with the remarkably large Stokes shifts of up to 7700 cm^{-1}, suggest that such *block*-type π-conjugated materials could prove broadly useful in applications ranging from cellular imaging to supramolecular assembly.

Acknowledgements

This work was supported by the National Natural Science Foundation of China (NSFC) (No. 21772012). F.J. thanks the US National Science Foundation (NSF) for support under Grant CHE-1954122. We are greatly thankful to Prof. Suning Wang at

Queen's University for helpful discussions over the years. We thank Dr. Pavel Kucheryavy at Rutgers University-Newark for assistance with variable temperature ^{11}B NMR spectroscopy data acquisition. We thank the Analysis & Testing Center at Beijing Institute of Technology for advanced facilities.

Conflict of Interest

The authors declare no conflict of interest.

Keywords: Boron • Conjugated Macrocycles • Donor-Acceptor Blocks • Luminescence • Optoelectronic

[1] a) Z. Liu, S. K. M. Nalluri, J. F. Stoddart, *Chem. Soc. Rev*. **2017**, *46*, 2459–2478; b) P. Neri, J. L. Sessler, M.-X. Wang, Springer: Switzerland, **2016**; c) D. Xia, P. Wang, X. Ji, N. M. Khashab, J. L. Sessler, F. Huang, *Chem. Rev*. **2020**, *120*, 6070–6123; d) D. S. Kim, J. L. Sessler, *Chem. Soc. Rev*. **2015**, *44*, 532–546; e) X. Ma, Y. Zhao, *Chem. Rev*. **2015**, *115*, 7794–7839.

[2] a) M. G. T. A. Rutten, F. W. Vaandrager, J. A. A. W. Elemans, R. J. M. Nolte, *Nat. Rev. Chem*. **2018**, *2*, 365–381; b) M. Iyoda, J. Yamakawa, M. J. Rahman, *Angew. Chem., Int. Ed*. **2011**, *50*, 10522–10553; *Angew. Chem*. **2011**, *123*, 10708–10740; c) R. Chakrabarty, P. S. Mukherjee, P. J. Stang, *Chem. Rev*. **2011**, *111*, 6810–6918; d) J.-M. Lehn, *Science* **1993**, *260*, 1762–1764; e) F. Picini, S. Schneider, O. Gavat, A. V. Jentzsch, J. Tan, M. Maaloum, J.-M. Strub, S. Tokunaga, J.-M. Lehn, E. Moulin, N. Giuseppone, *J. Am. Chem. Soc*. **2021**, *143*, 6498–6504.

[3] a) Y. Wang, H. Wu, J. F. Stoddart, *Acc. Chem. Res*. **2021**, *54*, 2027–2039; b) D. B. Smith, D. K. Amabilino, J. W. Steed, *Chem. Soc. Rev*. **2017**, *46*, 2404–2420; c) E. Busseron, Y. Ruff, E. Moulin, N. Giuseppone, *Nanoscale* **2013**, *5*, 7098–7140; d) Y. Segawa, D. R. Levine, K. Itami, *Acc. Chem. Res*. **2019**, *52*, 2760–2767; e) T. Kawase, H. Kurata, *Chem. Rev*. **2006**, *106*, 5250–5273; f) K. Tahara, Y. Tobe, *Chem. Rev*. **2006**, *106*, 5274–5290.

[4] a) C. Liu, Y. Ni, X. Lu, G. Li, J. Wu, *Acc. Chem. Res*. **2019**, *52*, 2309–2321; b) M. Iyoda, H. Shimizu, *Chem. Soc. Rev*. **2015**, *44*, 6411–6424; c) M. Ball, B. Zhang, Y. Zhong, B. Fowler, S. Xiao, F. Ng, M. Steigerwald, C. Nuckolls, *Acc. Chem. Res*. **2019**, *52*, 1068–1078; d) H. Osaki, C.-M. Chou, M. Taki, K. Welke, D. Yokogawa, S. Irle, Y. Sato,T. Higashiyama, S. Saito, A. Fukazawa, S. Yamaguchi, *Angew. Chem., Int. Ed*. **2016**, *55*, 7131–7135; *Angew. Chem*. **2016**, *128*, 7247–7251.

[5] a) M. Hirai, N. Tanaka, M. Sakai, S. Yamaguchi, *Chem. Rev*. **2019**, *119*, 8291–8331; b) M. Stępień, E. Gońka, M. Żyła, N. Sprutta, *Chem. Rev*. **2017**, *117*, 3479–3716; c) X. Su, T. A. Bartholome, J. R. Tidwell, A. Pujol, S. Yruegas, J. J. Martinez, C. D. Martin, *Chem. Rev*. **2021**, *121*, 4147–4192; d) X.-Y. Wang, F.-D. Zhuang, R.-B. Wang, X.-C. Wang, X.-Y. Cao, J.-Y. Wang, J. Pei, *J. Am. Chem. Soc*. **2014**, *136*, 3764–3767; e) D.-T. Yang, S. K. Mellerup, J.-B. Peng, X. Wang, Q.-S. Li, S. Wang, *J. Am. Chem. Soc*. **2016**, *138*, 11513–11516; f) N. Ando, T. Yamada, H. Narita, N. N. Oehlmann, M. Wagner, S. Yamaguchi, *J. Am. Chem. Soc*. **2021**, *143*, 9944–9951; g) A. S. Scholz, J. G. Massoth, M. Bursch, J.-M. Mewes, T. Hetzke, B. Wolf, M. Bolte, H.-W. Lerner, S. Grimme, M. Wagner, *J. Am. Chem. Soc*. **2020**, *142*, 11072–11083; h) K. Yang, G. Zhang, Q. Song, *Chem. Sci*. **2018**, *9*, 7666–7672; i) Y. Fu, H. Yang, Y. Gao, L. Huang, R. Berger, J. Liu, H. Lu, Z. Cheng, S. Du, H.-J. Gao, X. Feng, *Angew. Chem., Int. Ed*. **2020**, *59*, 8873–8879; *Angew. Chem*. **2020**, *132*, 8958–8964; j) A. Ito, M. Uebe, R. Kurata, S. Yano, H. Fueno, T. Matsumoto, *Chem. Asian J*. **2018**, *13*, 754–760; k) J.-F. Chen, X. Yin, B. Wang, K. Zhang, G. Meng, S. Zhang, Y. Shi, N. Wang, S. Wang, P. Chen, *Angew. Chem., Int. Ed*. **2020**, *59*, 11267–11272; *Angew. Chem*. **2020**, *132*, 11363–11368; l) Q. Hou, L. Liu, S. K. Mellerup, N. Wang, T. Peng, P. Chen, S. Wang, *Org. Lett*. **2018**, *20*, 6467–6470; m) F. Vidal, F. Jäkle, *Angew. Chem. Int. Ed*. **2019**, *58*, 5846–5870; *Angew. Chem*. **2019**, *131*, 5904–5929; n) Z. Huang, S. Wang, R. D. Dewhurst, N. V. Ignat'ev, M. Finze, H. Braunschweig, *Angew. Chem. Int. Ed*. **2020**, *59*, 8800–8816; *Angew. Chem*. **2020**, *132*, 8882–8900; o) A. G. Bonn, O. S. Wenger, *J. Org. Chem*. **2015**, *80*, 4097–4107; p) C. D. Entwistle, T. B. Marder, *Angew. Chem. Int. Ed*. **2002**, *41*, 2927–2931; *Angew. Chem*. **2002**, *116*, 3051–3056.

[6] a) P. Chen, X. Yin, N. Baser-Kirazli, F. Jäkle, *Angew. Chem., Int. Ed*. **2015**, *54*, 10768–1077; *Angew. Chem*. **2015**, *127*, 10918–10922; b) N. Baser-Kirazli, R. A. Lalancette, F. Jäkle, *Organometallics* **2021**, *40*, 520–528; c) H. C. Schmidt, L. G. Reuter, J. Hamacek, O. S. Wenger, *J. Org. Chem*. **2011**, *76*, 9081–9085; d) L. Weber, D. Eickhoff, T. B. Marder, M. A. Fox, P. J. Low, A. D. Dwyer, D. J. Tozer, S. Schwedler, A. Brockhinke, H.-G. Stammler, B. Neumann, *Chem.–Eur. J*. **2012**, *18*, 1369–1382; e) X. Y. Liu, D. R. Bai, S. Wang, *Angew. Chem., Int. Ed*. **2006**, *45*, 5475–5478; *Angew. Chem*. **2006**, *118*, 5601–5604; f) A. Proń, M. Baumgarten, K. Müllen, *Org. Lett*. **2010**, *12*, 4236–4239; g) Z.-B. Sun, J.-K. Liu, D.-F. Yuan, Z.-H. Zhao, X.-Z. Zhu, D.-H. Liu, Q. Peng, C.-H. Zhao, *Angew. Chem., Int. Ed*. **2019**, *58*, 4840–4846; *Angew. Chem*. **2019**, *131*, 4894–4900; h) B. Adelizzi, P. Chidchob, N. Tanaka, B. A. G. Lamers, S. C. J. Meskers, S. Ogi, A. R. A. Palmans, S. Yamaguchi, E. W. Meijer, *J. Am. Chem. Soc*. **2020**, *142*, 16681–16689; i) D. Shimoyama, N. Baser-Kirazli, R. A. Lalancette, F. Jäkle, *Angew. Chem., Int. Ed*. **2021**, 60, 17942–17946; *Angew. Chem*. **2021**, *133*, 18086–18090; j) H. Helten, *Chem. Asian J*. **2020**, *15*, 915–919; k) L. Fritze, M. Fest, A. Helbig, T. Bischof, I. Krummenacher, H. Braunschweig, M. Finze, H. Helten, *Macromolecules* **2021**, *54*, 7653–7665; l) F. P. Gabbaï, *Angew. Chem., Int. Ed*. **2012**, *51*, 6316–6318; *Angew. Chem*. **2012**, *124*, 6423–6425; m) E. von Grotthuss, A. John, T. Kaese, M. Wagner, *Chem. Asian J*. **2018**, *7*, 37–53; n) A. Lorbach, A. Hübner, M. Wagner, *Dalton Trans*. **2012**, *41*, 6048–6063; o) K. Schickedanz, J. Radtke, M. Bolte, H. Lerner, M. Wagner, *J. Am. Chem. Soc*. **2017**, *139*, 2842–2851; p) R. Hu, E. Lager, A. Aguilar-Aguilar, J. Liu, J. W. Y. Lam, H. H. Y. Sung, I. D. Williams, Y. Zhong, K. S. Wong, E. Peña-Cabrera, B. Z. Tang, *J. Phys. Chem. C* **2009**, *113*, 15845–15853.

[7] A. Ito, Y. Yokoyama, R. Aihara, K. Fukui, S. Eguchi, K. Shizu, T. Sato, K. Tanaka, *Angew. Chem., Int. Ed*. **2010**, *49*, 8205–8208; *Angew. Chem*. **2010**, *122*, 8381–8384.

[8] a) P. Chen, F. Jäkle, *J. Am*. Chem. Soc. **2011**, *133*, 20142–20145; b) N. Baser-Kirazli, R. A. Lalancette, F. Jäkle, *Angew. Chem., Int. Ed*. **2020**, *59*, 8689–8697; *Angew. Chem*. **2020**, *132*, 8767–8775; c) P. Chen, R. A. Lalancette, F. Jäkle, *Angew. Chem., Int. Ed*. **2012**, *51*, 7994–7998; *Angew. Chem*. **2012**, *124*, 8118–8122.

[9] a) H. Wei, Y. Liu, T. Y. Gopalakrishna, H. Phan, X. Huang, L. Bao, J. Guo, J. Zhou, S. Luo, J. Wu, Z. Zeng, *J. Am. Chem. Soc*. **2017**, *139*, 15760–15767; b) H.-Y. Zhang, Y.-Y. Tang, P.-P. Shi, R.-G. Xiong, *Acc. Chem. Res*. **2019**, *52*, 1928–1938; c) S. Horiuchi, Y. Tokura, *Nat. Mater*. **2008**, *7*, 357–366; d) J. Wudarczyk, G. Papamokos, V. Margaritis, D. Schollmeyer, F. Hinkel, M. Baumgarten, G. Floudas, K. Müllen, *Angew. Chem., Int. Ed*. **2016**, *55*, 1–5; *Angew. Chem*. **2016**, *128*, 3275–3278; e) S. Furukawa, J. Wu, M. Koyama, K. Hayashi, N. Hoshino, T. Takeda, Y. Suzuki, J. Kawamata, M. Saito, T. Akutagawa, *Nat. Commun*. **2021**, *12*, 768.

[10] a) L. Ji, S. Griesbeck, T. B. Marder, *Chem. Sci*. **2017**, *8*, 846–863; b) C. R. Wade, A. E. J. Broomsgrove, S. Aldridge, F. P. Gabbai, *Chem. Rev*. **2010**, *110*, 3958–3984; c) Z. Yuan, J. C. Collings, N. J. Taylor, T. B. Marder, C. Jardin, J.-F. Halet, *J. Solid State Chem*. **2000**, *154*, 5–12; d) S. Griesbeck, E. Michail, C. Wang, H. Ogasawara, S. Lorenzen, L. Gerstner, T. Zang, J. Nitsch, Y. Sato, R. Bertermann, M. Taki, C. Lambert, S. Yamaguchi, T. B. Marder, *Chem. Sci*. **2019**, *10*, 5405–5422; e) Y. Wang, H. Wu, P. Li, S. Chen, L. O. Jones, M. A. Mosquera, L. Zhang, K. Cai, H. Chen, X.-Y. Chen, C. L. Stern, M. R. Wasielewski, M. A. Ratner, G. C. Schatz, J. F. Stoddart, *Nat. Commun*. **2020**, *11*, 4633; f) H. M. Kim, B. R. Cho, *Chem. Rev*. **2015**, *115*, 5014–5055.

[11] a) K. Matsui, S. Oda, K. Yoshiura, K. Nakajima, N. Yasuda, T. Hatakeyama, *J. Am. Chem. Soc*. **2018**, *140*, 1195–1198; b) Y. Zhang, D. Zhang, J. Wei, Z. Liu, Y. Lu, L. Duan, *Angew. Chem., Int. Ed*. **2019**, *58*, 16912–16917; *Angew. Chem*. **2019**, 131, 17068–17073; c) R. Zhao, J. Liu, L. Wang, *Acc. Chem. Res*. **2020**, *53*, 1557–1567; d) H. Uoyama, K. Goushi, K. Shizu, H. Nomura, C. Adachi, *Nature* **2012**, *492*, 234–240.

[12] For similar phenomena, see: R. Rulkens, A. J. Lough, I. Manners, *J. Am. Chem. Soc*. **1994**, *116*, 797-798.

[13] Incomplete recovery of **MC**-*b*-**B3N3** and **L**-*b*-**B3N3** upon water treatment may be due to the biphasic reaction conditions (toluene/H_2O), and could also be related to partial hydrolysis of the resulting fluoroborates.

Entry for the Table of Contents

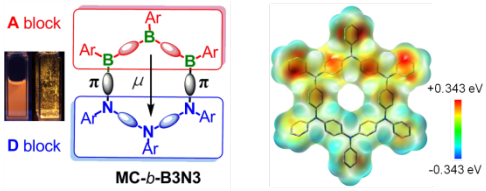

An unusual *block*-type π-conjugated macrocycle **MC**-*b*-**B3N3** that shows a strong dipole moment and a narrow HOMO-LUMO gap is introduced. Compared with other cyclic hexamers, its unique orientation of electron-donor block and acceptor block resulted in largely red-shifted orange emission both in solution and in the solid state.